INTERNATIONAL JOURNAL FOR NUMERICAL METHODS IN ENGINEERING
Int. J. Numer. Meth. Engng 2003; **57**:1177–1196 (DOI: 10.1002/nme.824)

Topology optimization with implicit functions and regularization

T. Belytschko*,†, S. P. Xiao and C. Parimi

Department of Mechanical Engineering, 2145 N. Sheridan Road, Northwestern University, Evanston, IL 60208, U.S.A.

SUMMARY

Topology optimization is formulated in terms of the nodal variables that control an implicit function description of the shape. The implicit function is constrained by upper and lower bounds, so that only a band of nodal variables needs to be considered in each step of the optimization. The weak form of the equilibrium equation is expressed as a Heaviside function of the implicit function; the Heaviside function is regularized to permit the evaluation of sensitivities. We show that the method is a dual of the Bendsøe–Kikuchi method. The method is applied both to problems of optimizing single material and multi-material configurations; the latter is made possible by enrichment functions based on the extended finite element method that enable discontinuous derivatives to be accurately treated within an element. The method is remarkably robust and we found no instances of checkerboarding. The method handles topological merging and separation without any apparent difficulties. Copyright © 2003 John Wiley & Sons, Ltd.

KEY WORDS: topology optimization; implicit function

1. INTRODUCTION

This paper presents a new approach to topology optimization based on implicit functions. The implicit functions are approximated by the same mesh and shape functions that are used for the solution of the equilibrium equations. The shape is then piecewise continuously differentiable, although it is also feasible to use Hermite interpolants for the implicit function and obtain continuously differentiable shapes.

A key step in the method is that the equilibrium equations are expressed in the design space with the current topology expressed by a Heaviside step function. This step function

*Correspondence to: T. Belytschko, Department of Mechanical Engineering, 2145 N. Sheridan Road, Northwestern University, Evanston, IL 60208, U.S.A.
†E-mail: tedbelytschko@northwestern.edu

Contract/grant sponsor: National Aeronautics and Space Administration (NASA)

Received 4 November 2002
Revised 9 December 2002
Accepted 21 January 2003

Copyright © 2003 John Wiley & Sons, Ltd.

is then regularized to enable sensitivity matrices (derivatives of the objective functions and constraints) to be evaluated.

The method is linked to the extended finite element method [1, 2]. This enables the design to include features such as interfaces between materials that are not coincident with the mesh, arbitrarily positioned cracks, holes, etc. Although only examples of the use of interfaces are given here, the resulting method has the potential to treat problems of optimal design that have not been treated before. The method is remarkably robust and mesh-independent. In the problems we have run, we find no evidence of checkerboarding or any other instability. Furthermore, so-called grayscale subdomains are avoided and mesh-dependence appears to be minimal.

The modern theory of structural optimization was developed by Schmit [3], Fox [4] and Prager and Taylor [5] in the 1960s. It was mainly aimed in sizing problems of frame structures [6, 7]. Shape optimization is reported in Zienkiewicz and Campbell [8], a survey of early works can be found in Reference [9].

In the pioneering work of Bendsøe and Kikuchi [10], a so-called microstructure or homogenization based approach was developed for topology optimization problems. In Reference [10], the design space is covered by a structured mesh of finite elements, usually of low order. The optimization problem is then posed as finding the parameters of elements where the parameters are based on a microstructure of the material in these elements. The parameters usually characterize the sizes of holes in the microstructure, so the outcome of the optimization procedure is that most elements are filled or empty. The outline of the filled elements then constitutes the optimum topology. Incidentally, it is our opinion that the microstructural model acts primarily as a regularization of the empty-filled (0-1) problem.

This is borne out by the so-called inverse homogenization approach of Bendsøe [11], also see References [12, 13]. In this approach, the 0-1 condition for each element is regularized by multiplying the integrands in the problem by ρ^{α}, where generally $\alpha \geqslant 3$. This again regularizes the (0-1) transition of an element from empty to full. The regularization occurs primarily for $\rho = 0$, but at the other end of the interval a constraint is used. Note that while the requirement $\alpha \geqslant 3$ is often attributed to microstructural considerations, it is the lowest value of α for which the second derivative is continuous at $\rho = 0$.

We will not review the extensive literature on various material interpolation schemes; an extensive bibliography can be found for example in Bendsøe [14] and Sigmund [15].

The only recent method that is similar to this paper is by Sethian and Wiegmann [16], who use level set methods. Level set methods are also based on implicit functions, but employ the integration of hyperbolic conservation equations to update the implicit functions.

The approach given here differs in several respects from the method of Sethian and Wiegmann [16]. Since a weak form of the equilibrium equations is used here, the topology can be explicitly incorporated in the equilibrium constraint by a Heaviside function of the implicit function that describes the shape. Therefore, neither the development of relations between stress and velocity nor the integration of conservation equations is needed in our approach. Secondly, a finite element method is used instead of a finite difference method. While the choice between the finite element and finite difference methods is perhaps primarily a matter of personal preference, the finite element method does facilitate the use of unstructured meshes, which is sometimes desirable. Furthermore, the overall treatment of discontinuities and interfaces with any order of accuracy appears to be substantially more straightforward in the context of the extended finite element method used here.

Copyright © 2003 John Wiley & Sons, Ltd.

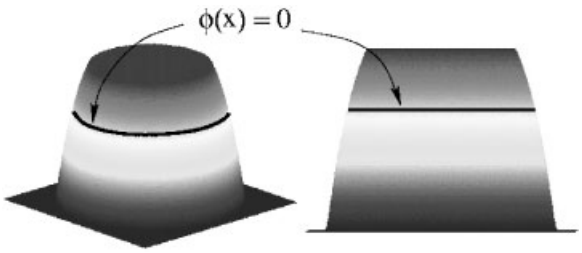

Figure 1. Constrained implicit function $\boldsymbol{\phi}(\mathbf{x})$.

The outline of this paper is as follows. In Section 2, the optimization problem is described. The discrete equations are obtained in Section 3. Section 4 examines the duality of this scheme with the Bendsøe–Kikuchi method. In Section 5, the optimization problem for composite materials is developed. Several examples including the topology optimization of composite materials are studied in Section 6, followed by the conclusions.

2. OPTIMIZATION PROBLEM

In the following, we present the formulation of the optimization problem. Small deformation elastic behaviour is considered here. We assume that we are given a design space Ω_{des} to which all possible designs are restricted. We seek a body Ω with boundary Γ that provides an optimal design. The topological design is described by an implicit function $\boldsymbol{\phi}(\mathbf{x})$ so that

$$\begin{aligned} &\boldsymbol{\phi}(\mathbf{x}) = 0 \quad \text{on } \Gamma \\ &\boldsymbol{\phi}(\mathbf{x}) > 0 \quad \text{inside } \Omega \\ &\boldsymbol{\phi}(\mathbf{x}) < 0 \quad \text{outside } \Omega \end{aligned} \tag{1}$$

The implicit function is initially chosen to be a signed distance function or defined by radial basis functions from a set of points; no effort is made to keep it a signed distance function during the optimization. The function $\boldsymbol{\phi}(\mathbf{x})$ is only considered of relevance in a narrow band about the surface $\boldsymbol{\phi}(\mathbf{x}) = 0$. Therefore, we impose the constraint

$$\text{if } |\boldsymbol{\phi}(\mathbf{x})| > \alpha \quad \text{then } \boldsymbol{\phi}(\mathbf{x}) = \alpha \ \text{sign}(\boldsymbol{\phi}(\mathbf{x})) \tag{2}$$

The resulting function then consists of two plateaus as shown in Figure 1 separated by a steep slope around the boundaries.

To clarify the subsequent developments, we consider the standard problem of minimizing the compliance C (maximizing the stiffness). Thus we seek in Ω_{des} the function $\boldsymbol{\phi}(\mathbf{x})$ which minimizes C subject to equilibrium and the volume constraint.

The mean compliance can be expressed as the following if body forces are not considered:

$$C = \int_{\Gamma_t} \mathbf{u}^{\mathrm{T}} \bar{\mathbf{t}} \, \mathrm{d}\Gamma \tag{3}$$

Copyright © 2003 John Wiley & Sons, Ltd.

where $\Gamma_{\mathbf{t}}$ is the surface on which the traction is prescribed to be $\bar{\mathbf{t}}$. The location of the prescribed traction boundary is considered fixed. To enforce equilibrium, we will use the weak form (i.e. the principle of virtual work), which gives that for displacements $\mathbf{u} \in U$

$$\int_{\Omega_{\text{des}}} H(\boldsymbol{\phi}(\mathbf{x}))\delta\boldsymbol{\varepsilon}^{\mathrm{T}}\boldsymbol{\sigma}\,\mathrm{d}\Omega = \int_{\Gamma_t} \delta\mathbf{u}^{\mathrm{T}}\bar{\mathbf{t}}\,\mathrm{d}\Gamma \quad \forall\delta\mathbf{u} \in U_0 \tag{4}$$

where

$$H(\boldsymbol{\phi}(\mathbf{x})) = \begin{cases} 0 & \boldsymbol{\phi} < 0 \\ 1 & \boldsymbol{\phi} > 0 \end{cases} \tag{5}$$

In the above U and U_0 are the spaces of kinematically admissible displacements

$$U = \{\mathbf{u}(\mathbf{x}) | u_i(\mathbf{x}) \in C^0 \mid u_i = \bar{u}_i \text{ on } \Gamma_u\} \tag{6}$$

$$U_0 = \{\delta\mathbf{u}(\mathbf{x}) | \delta u_i(\mathbf{x}) \in C^0 \mid \delta u_i = 0 \text{ on } \Gamma_u\} \tag{7}$$

where C^0 denotes a space of piecewise continuously differentiable function, $\boldsymbol{\varepsilon}$ are the strains and $\boldsymbol{\sigma}$ the stresses; the prefix δ indicates a variation (or test function). Note that the displacement constraints are given in Equation (6). The shape of the structure has been embedded in the above weak form of the equilibrium equations by multiplying the integrand by $H(\boldsymbol{\phi}(\mathbf{x}))$ as in the structured version of X-FEM [17, 18] described in Reference [2].

For an elastic material (4) is equivalent to the principle of minimum potential energy

$$\mathbf{u} = \text{Arg}\left[\inf_{\mathbf{u}} \Pi(\mathbf{u})\right] \quad \mathbf{u} \in U \tag{8}$$

where

$$\Pi(\mathbf{u}) = \frac{1}{2}\int_{\Omega_{\text{des}}} H(\boldsymbol{\phi}(\mathbf{x}))\boldsymbol{\varepsilon}^{\mathrm{T}}\mathbf{C}\boldsymbol{\varepsilon}\,\mathrm{d}\Omega - \int_{\Gamma_t} \mathbf{u}^{\mathrm{T}}\bar{\mathbf{t}}\,\mathrm{d}\Gamma \tag{9}$$

and $\mathbf{C}$ is the elasticity matrix.

The volume constraint can be imposed as

$$g = \int_{\Omega_{\text{des}}} H(\boldsymbol{\phi}(\mathbf{x}))\,\mathrm{d}\Omega - V_0 = 0 \tag{10}$$

where V_0 is the specified volume. The design problem can then be posed as

$$\underset{\boldsymbol{\phi}}{\text{Minimize}}\ C(\boldsymbol{\phi}) \tag{11}$$

subject to the weak form of equilibrium (4), the displacement constraints in Equation (6) and the volume constraint (10).

We note that by the principle of minimum potential energy, the objective function can be written as

$$\Pi = \frac{1}{2}\int_{\Omega_{\text{des}}} H(\boldsymbol{\phi}(\mathbf{x}))\boldsymbol{\varepsilon}^{\mathrm{T}}\mathbf{C}\boldsymbol{\varepsilon}\,\mathrm{d}\Omega - C = \frac{1}{2}\int_{\Omega_{\text{des}}} H(\boldsymbol{\phi}(\mathbf{x}))\boldsymbol{\varepsilon}^{\mathrm{T}}\boldsymbol{\sigma}\,\mathrm{d}\Omega - \int_{\Gamma_t} \mathbf{u}^{\mathrm{T}}\bar{\mathbf{t}} \tag{12}$$

Copyright © 2003 John Wiley & Sons, Ltd.

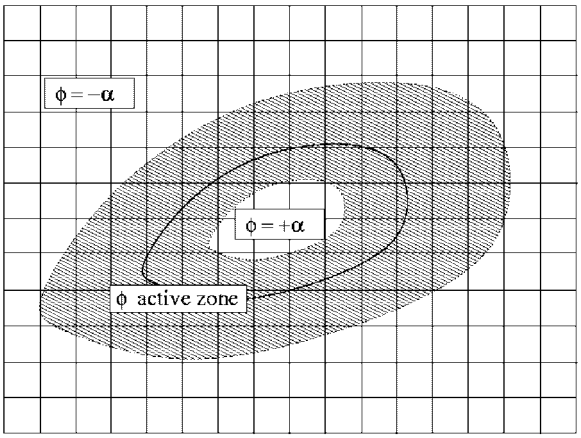

Figure 2. Narrow band for active $\boldsymbol{\phi}$ around boundary.

Therefore, the optimization problem can be posed as the max–min problem

$$\boldsymbol{\phi} = \text{Arg}\left\{\sup_{\boldsymbol{\phi}(\mathbf{x})}\left[\inf_{\mathbf{u}(\mathbf{x})} \Pi(\mathbf{u}(\mathbf{x}), \boldsymbol{\phi}(\mathbf{x}))\right]\right\} \tag{13}$$

subject to the displacement constraints and volume constraint.

3. DISCRETIZATION AND SOLUTION PROCEDURE

For the purpose of formulating the discrete problem, we approximate $\boldsymbol{\phi}(\mathbf{x})$ by shape functions $N_I(\mathbf{x})$.

$$\boldsymbol{\phi}^h(\mathbf{x}) = \sum_I N_I(\mathbf{x})\boldsymbol{\phi}_I \tag{14}$$

In most cases considered here the mesh is structured, but the method is applicable without modification to unstructured meshes. This is one of the key steps in the method: the geometry (or topology) is described by the nodal values of $\boldsymbol{\phi}(\mathbf{x})$ and shape functions so that the space of achievable designs will be C^0 in shape when C^0 shape functions are used. Smoother shapes can be obtained by using C^1 shape functions, which are not difficult to construct when the elements are rectangular. Corresponding to (2), the values of $\boldsymbol{\phi}_I$ are constrained by the rule

$$\text{if } |\boldsymbol{\phi}_I| > \alpha \quad \text{then } \boldsymbol{\phi}_I = \alpha\,\text{sign}(\boldsymbol{\phi}_I) \tag{15}$$

Therefore, only the nodal variables in a narrow band about the current boundary are considered unknowns in any step of the optimization. The implicit function definition is then as depicted in Figure 2. Around the boundary of the object, the nodal value of $\boldsymbol{\phi}(\mathbf{x})$ varies approximately linearly with the distance from the boundary. Beyond a certain distance, however, $\boldsymbol{\phi}$ becomes constant.

Copyright © 2003 John Wiley & Sons, Ltd.

The displacement field is similarly described by shape functions, so

$$\mathbf{u}^h(\mathbf{x}) = \sum_I N_I(\mathbf{x})\mathbf{u}_I \tag{16}$$

$$\delta\mathbf{u}^h(\mathbf{x}) = \sum_I N_I(\mathbf{x})\delta\mathbf{u}_I \tag{17}$$

Therefore, from (4) the equilibrium equations can be written as

$$\int_{\Omega_{\text{des}}} H(\boldsymbol{\phi}(\mathbf{x}))\mathbf{B}_I\boldsymbol{\sigma}\,\mathrm{d}\Omega = \int_{\Gamma_t} N_I\,\mathbf{t}\,\mathrm{d}\Gamma \tag{18}$$

where $\mathbf{B}_I$ are submatrices of the standard strain-displacement matrix $\mathbf{B}$ that gives $\boldsymbol{\varepsilon}$ by

$$\boldsymbol{\varepsilon} = \sum_I \mathbf{B}_I\mathbf{u}_I = \mathbf{B}\mathbf{u} \tag{19}$$

and the displacement and volume constraints can be written as

$$\begin{aligned} \mathbf{g}^u &= \{g_i^u\} = \{u_i(\mathbf{x}) - \bar{u}_i(\mathbf{x})\} = \left\{\sum_J N_J(\mathbf{x})u_{iJ} - \bar{u}_i(\mathbf{x})\right\} = 0 \\ g^v &= \int_{\Omega_{\text{des}}} H(\boldsymbol{\phi})\,\mathrm{d}\Omega - V_0 = 0 \end{aligned} \tag{20}$$

The objective function (12) with respect to the displacements can be written as the following by means of the augmented Lagrangian method for the displacement constraints:

$$\begin{aligned} W_{AL}(\mathbf{u}_I, \boldsymbol{\lambda}_1) &= \Pi + \boldsymbol{\lambda}_1^{\mathrm{T}}\mathbf{g}^u + \frac{1}{2}p\mathbf{g}^{u^{\mathrm{T}}}\mathbf{g}^u \\ &= \frac{1}{2}\int_{\Omega_{\text{des}}} H(\boldsymbol{\phi}(\mathbf{x}))\boldsymbol{\varepsilon}^{\mathrm{T}}\mathbf{C}\boldsymbol{\varepsilon}\,\mathrm{d}\Omega - C + \boldsymbol{\lambda}_1^{\mathrm{T}}\mathbf{g}^u + \frac{1}{2}p\mathbf{g}^{u^{\mathrm{T}}}\mathbf{g}^u \end{aligned} \tag{21}$$

where $\boldsymbol{\lambda}_1$ is a vector of the Lagrange multipliers and p is the penalty parameter.

Similarly the objective functions with respect to the implicit function can be expressed as the following by means Lagrange multiplier method for the volume constraint:

$$\begin{aligned} \Pi_L(\boldsymbol{\phi}_I, \lambda_2) &= \Pi + \lambda_2 g^v \\ &= \frac{1}{2}\int_{\Omega_{\text{des}}} H(\boldsymbol{\phi}(\mathbf{x}))\boldsymbol{\varepsilon}^{\mathrm{T}}\mathbf{C}\boldsymbol{\varepsilon}\,\mathrm{d}\Omega - C + \lambda_2 g^v \\ &= -\frac{1}{2}\int_{\Omega_{\text{des}}} H(\boldsymbol{\phi}(\mathbf{x}))\boldsymbol{\varepsilon}^{\mathrm{T}}C\boldsymbol{\varepsilon}\,\mathrm{d}\Omega + \lambda_2 g^v \end{aligned} \tag{22}$$

where λ_2 is a scalar Lagrange multiplier for the volume constraint.

The optimization problem is solved by the following iterative procedure:

1. Minimize the potential function $W_{AL}(\mathbf{u}_I, \boldsymbol{\lambda}_1)$ in (21) to obtain the equilibrium displacements $\mathbf{u}_I$.

Copyright © 2003 John Wiley & Sons, Ltd.

2. Maximize the objective function $\Pi_L(\boldsymbol{\phi}_I, \boldsymbol{\lambda}_2)$ in (22) to update the nodal value of the implicit function $\boldsymbol{\phi}_I$.

The first step can be solved by using the CG (conjugate gradient) method, Fletcher *et al.* [19]. The equilibrium displacement for any $\boldsymbol{\phi}_I$ is the stationary point of $W_{AL}(\mathbf{u}_I, \boldsymbol{\lambda}_1)$, i.e. the point where the first derivatives of $W_{AL}(\mathbf{u}_I, \boldsymbol{\lambda}_1)$ vanish with respect to $\mathbf{u}_I$ and $\boldsymbol{\lambda}_1$, respectively. The discrete equations are:

$$\frac{\partial W_{AL}}{\partial \mathbf{u}_I} = \int_{\Omega_{\text{des}}} H(\boldsymbol{\phi}(\mathbf{x})) \frac{\partial \boldsymbol{\varepsilon}^{\mathrm{T}}}{\partial \mathbf{u}_I} \mathbf{C} \boldsymbol{\varepsilon} \, \mathrm{d}\Omega - \int_{\Gamma_t} \bar{\mathbf{t}} \cdot \frac{\partial \mathbf{u}(\mathbf{x})}{\partial \mathbf{u}_I} \, \mathrm{d}\Gamma + \boldsymbol{\lambda}_1^{\mathrm{T}} \frac{\partial \mathbf{g}^u}{\partial \mathbf{u}_I} + p \left[\frac{\partial \mathbf{g}^u}{\partial \mathbf{u}_I} \right]^{\mathrm{T}} \mathbf{g}^u = 0 \tag{23}$$

$$\frac{\partial W_{AL}}{\partial \boldsymbol{\lambda}_1} = \mathbf{g}^u = \{u_i - \bar{u}_i\} = \left\{ \sum_J N_J u_{iJ} - \bar{u}_i \right\} = 0 \tag{24}$$

After the equilibrium displacement is obtained for current $\boldsymbol{\phi}_I$, the nodal values of the implicit function $\boldsymbol{\phi}_I$ are updated by maximizing the objective function $\Pi_L(\boldsymbol{\phi}_I, \boldsymbol{\lambda}_2)$. This corresponds to finding the point where the first derivatives of $\Pi_L(\boldsymbol{\phi}_I, \boldsymbol{\lambda}_2)$ vanish with respect to $\boldsymbol{\phi}_I$ and $\boldsymbol{\lambda}_2$:

$$\frac{\partial \Pi_L}{\partial \boldsymbol{\phi}_I} = -\frac{1}{2} \int_{\Omega_{\text{des}}} \frac{\partial H(\boldsymbol{\phi}(\mathbf{x}))}{\partial \boldsymbol{\phi}_I} \boldsymbol{\varepsilon}^{\mathrm{T}} \mathbf{C} \boldsymbol{\varepsilon} \, \mathrm{d}\Omega + \boldsymbol{\lambda}_2 \int_{\Omega_{\text{des}}} \frac{\partial H(\boldsymbol{\phi}(\mathbf{x}))}{\partial \boldsymbol{\phi}_I} \, \mathrm{d}\Omega = 0 \tag{25}$$

$$\frac{\partial \Pi_L}{\partial \boldsymbol{\lambda}_2} = g^v = \int_{\Omega_{\text{des}}} H(\boldsymbol{\phi}(\mathbf{x})) \, \mathrm{d}\Omega - V_0 = 0 \tag{26}$$

However, the first derivatives of the objective functions involve derivatives with respect to arguments of the step functions, $H(\boldsymbol{\phi})$. Since the derivative of the Heaviside step function is the Dirac delta function, it would make the method unworkable. Therefore we regularize the step function so that its derivative can be obtained numerically. We use different regularized functions for the weak equilibrium equation and the volume constraint. The regularized step functions for weak equilibrium and volume are, respectively

$$\text{equilibrium: } \bar{H}_1(\boldsymbol{\phi}) = \begin{cases} \Delta & \boldsymbol{\phi} \leqslant -l \\ \dfrac{1}{4}\left(1 + \sin \dfrac{\pi \boldsymbol{\phi}}{2l}\right)^2 & -l < \boldsymbol{\phi} < l \\ 1 & \boldsymbol{\phi} \geqslant l \end{cases} \tag{27}$$

$$\text{volume: } \bar{H}_2(\boldsymbol{\phi}) = \begin{cases} \Delta & \boldsymbol{\phi} \leqslant -l \\ \dfrac{1}{2}\left(1 + \sin \dfrac{\pi \boldsymbol{\phi}}{2l}\right) & -l < \boldsymbol{\phi} < l \\ 1 & \boldsymbol{\phi} \geqslant l \end{cases} \tag{28}$$

where l is the smoothing length and $l \leqslant \alpha$, Δ is a small positive number to ensure that the numerical stiffness for any design in the design domain is non-singular. These regularized step functions and their derivatives are shown in Figure 3. It can be seen that $\bar{H}_2(\boldsymbol{\phi})$ is smoother than $\bar{H}_1(\boldsymbol{\phi})$. Note the volume step function regularization is only used for (25) not (26).

Copyright © 2003 John Wiley & Sons, Ltd.

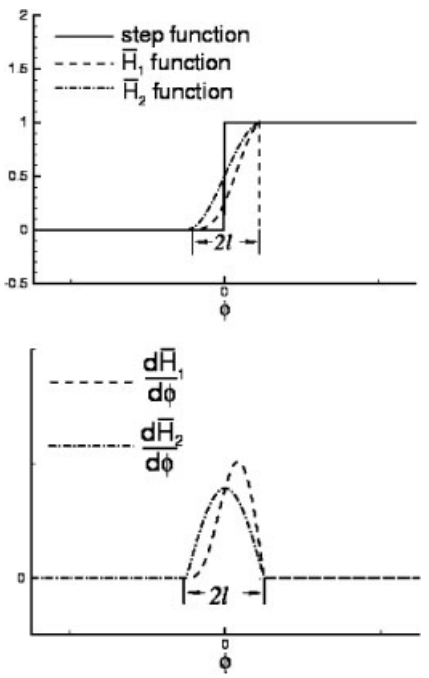

Figure 3. Regularized (smoothed) step functions $\bar{H}(\boldsymbol{\phi})$ and their derivatives $\bar{H}'$ (regularized Dirac delta functions).

Replacing the step functions by (27) and (28), the discrete equations (23) and (24) can be written as

$$\frac{\partial W_{AL}}{\partial \mathbf{u}_I} = \int_{\Omega_{\text{des}}} \bar{H}_1(\boldsymbol{\phi}(\mathbf{x}))\mathbf{B}_I^{\mathrm{T}}\boldsymbol{\sigma}\,\mathrm{d}\Omega - \int_{\Gamma_t} N_I\bar{\mathbf{t}}\,\mathrm{d}\Gamma + \boldsymbol{\lambda}_1^{\mathrm{T}}\mathbf{G}_I + p\mathbf{G}_I\mathbf{g}^u = 0 \tag{29}$$

$$\frac{\partial W_{AL}}{\partial \boldsymbol{\lambda}_1} = \mathbf{g}^u = \{u_i - \bar{u}_i\} = \left\{\sum_J N_J u_{iJ} - \bar{u}_i\right\} = 0 \tag{30}$$

where $\mathbf{G}_I = \{\partial \mathbf{g}^u/\partial \mathbf{u}_I\} = \{G_{ij}\}_I = \{\partial \mathbf{g}_j^u/\partial u_i\}_I = \{N_J\delta_{IJ}\delta_{ij}\}$

The conjugate gradient method with the secant method is used to solve the above equations. The secant method is used because it avoids calculating the second derivatives of function W_{AL} to obtain the stationary point of W_{AL}.

Similarly, (25) and (26) can then be written as

$$\begin{aligned}\frac{\partial \Pi_L}{\partial \boldsymbol{\phi}_I} &= -\frac{1}{2}\int_{\Omega_{\text{des}}} \frac{\partial \bar{H}_1(\boldsymbol{\phi}(\mathbf{x}))}{\partial \boldsymbol{\phi}_I}\boldsymbol{\varepsilon}^{\mathrm{T}}\boldsymbol{\sigma}\,\mathrm{d}\Omega + \boldsymbol{\lambda}_2\int_{\Omega_{\text{des}}} \frac{\partial \bar{H}_2(\boldsymbol{\phi}(\mathbf{x}))}{\partial \boldsymbol{\phi}_I}\,\mathrm{d}\Omega \\ &= -\frac{1}{2}\int_{\Omega_{\text{des}}} \bar{H}_1'(\boldsymbol{\phi})N_I(\boldsymbol{\phi}(\mathbf{x}))\boldsymbol{\varepsilon}^{\mathrm{T}}\boldsymbol{\sigma}\,\mathrm{d}\Omega + \boldsymbol{\lambda}_2\int_{\Omega_{\text{des}}} \bar{H}_2'(\boldsymbol{\phi})N_I(\boldsymbol{\phi}(\mathbf{x}))\,\mathrm{d}\Omega \\ &= 0\end{aligned} \tag{31}$$

Copyright © 2003 John Wiley & Sons, Ltd.

$$\frac{\partial \Pi_L}{\partial \boldsymbol{\lambda}_2} = g^v = \int_{\Omega_{\text{des}}} H(\boldsymbol{\phi}(\mathbf{x}))\,\mathrm{d}\Omega - V_0 = 0 \tag{32}$$

where we have used the following

$$\frac{\partial}{\partial \boldsymbol{\phi}_I} \bar{H}_i \left(\sum_J \boldsymbol{\phi}_J N_J \right) = \bar{H}_i'(\boldsymbol{\phi}) N_I(\mathbf{x}) \tag{33}$$

and $\bar{H}_i'(\boldsymbol{\phi})$ is the derivative of $\bar{H}_i(\boldsymbol{\phi})$ with respect to its argument.

Following Bendsøe [14] we use a heuristic updating scheme for the nodal values of the implicit function $\boldsymbol{\phi}_I$. The update formula is

$$\boldsymbol{\phi}_I^{\text{new}} = (\boldsymbol{\phi}_I + \alpha) A_I^{\eta} - \alpha \tag{34}$$

where η is an exponent that serves as a numerical damping coefficient; we use $\eta = 0.5$; A_I is given by

$$A_I = \frac{\displaystyle\int_{\Omega_{\text{des}}} \bar{H}_1'(\boldsymbol{\phi}) N_I(\boldsymbol{\phi}(\mathbf{x})) \boldsymbol{\varepsilon}^{\mathrm{T}} \mathbf{C} \boldsymbol{\varepsilon}\,\mathrm{d}\Omega}{\boldsymbol{\lambda}_2 \displaystyle\int_{\Omega_{\text{des}}} \bar{H}_2' N_I(\boldsymbol{\phi}(\mathbf{x}))\,\mathrm{d}\Omega} \tag{35}$$

We use bisection to determine the value of Lagrange multiplier $\boldsymbol{\lambda}_2$ which satisfies the volume constraint (32). Note that there is no smoothed step function in (32) so that the volume constraint is met exactly. The element integral in (32) is evaluated as described in Reference [2]. In some steps of the iterative process, all $\boldsymbol{\phi}_I$ for which $\boldsymbol{\phi}_I > 0$ should be considered in the optimization process. Otherwise, it may be possible that holes are missed. However, we only used $\boldsymbol{\phi}_I$ in a narrow band in most steps.

4. DUALITY

We can show that the proposed formulation is (with slight modification) a dual of the SIMP method. In the SIMP method the internal energy is written as

$$W^{\text{int}} = \frac{1}{2} \int_{\Omega_{\text{des}}} \rho^{\alpha} H(\rho) \boldsymbol{\varepsilon}^{\mathrm{T}} \boldsymbol{\sigma}\,\mathrm{d}\Omega \tag{36}$$

where ρ is a density; the step function is not included in the standard form of SIMP (e.g. see Sigmund [15]) but the equivalent constraint $\rho \geqslant 0$ is applied instead; if (36) is used, the constraint $\rho \geqslant 0$ is unnecessary. The volume constraint is similarly expressed in terms of a density. We can write (36) as

$$W^{\text{int}} = \frac{1}{2} \int_{\Omega_{\text{des}}} H(\boldsymbol{\phi}) \boldsymbol{\varepsilon}^{\mathrm{T}} \boldsymbol{\sigma}\,\mathrm{d}\Omega \tag{37}$$

where $\boldsymbol{\phi}$ is a generalized density function

$$\boldsymbol{\phi} = \rho^{\alpha} H(\rho) \tag{38}$$

Copyright © 2003 John Wiley & Sons, Ltd.

It can be seen that (37) is identical to the internal energy in (9) if we view $\boldsymbol{\phi}$ as a generalized density function.

The difference between the two methods lies in the interpolation of $\boldsymbol{\phi}$. In the proposed method, $\boldsymbol{\phi}(\mathbf{x})$ is interpolated by C^0 functions in terms of nodal variables, so

$$\boldsymbol{\phi}^{Nh}(\mathbf{x}) = \sum_I \boldsymbol{\phi}_I N_I(\mathbf{x}) \tag{39}$$

where $\boldsymbol{\phi}^{Nh}(\mathbf{x})$ refers to a nodal approximation of $\boldsymbol{\phi}(\mathbf{x})$.

In the Bendsøe–Kikuchi method and its offspring, $\boldsymbol{\phi}(\mathbf{x})$ is interpolated by an C^{-1} approximation in terms of element variables. Therefore, in general

$$\boldsymbol{\phi}^{Eh}(\mathbf{x}) = \sum_e \sum_\alpha \boldsymbol{\phi}_\alpha^e N_\alpha^e(\mathbf{x}) \tag{40}$$

where $\boldsymbol{\phi}^{Eh}(\mathbf{x})$ is an element-based approximation of $\boldsymbol{\phi}(\mathbf{x})$, $\boldsymbol{\phi}_\alpha^e = \boldsymbol{\phi}(\mathbf{x}_\alpha^e)$ and $\mathbf{x}_\alpha^e$ are a set of points in element e; $N_\alpha^e(\mathbf{x})$ are C^{-1} shape functions, so the support of $N_\alpha^e(\mathbf{x})$ is limited to element e. For constant $\boldsymbol{\phi}$ elements commonly used in topology optimization, the approximation is characterized by a single value in each element and (40) can be written as

$$\boldsymbol{\phi}^{Eh}(\mathbf{x}) = \sum_e \boldsymbol{\phi}^e H_e(\mathbf{x}) \tag{41}$$

where

$$H_e(\mathbf{x}) = \begin{cases} 1 & \text{if } \mathbf{x} \in \Omega_e \\ 0 & \text{if } \mathbf{x} \notin \Omega_e \end{cases} \tag{42}$$

The two approximations can be related by a least-square projection P so that

$$\boldsymbol{\phi}^{Nh} = \mathrm{P}\boldsymbol{\phi}^{Eh} \tag{43}$$

This projection is quite well known (see e.g. Reference [20, p. 36]). The nodal values of the C^0 function are given by

$$M_{IJ}\boldsymbol{\phi}_J = g_I \tag{44}$$

where

$$M_{IJ} = \int_\Omega N_I(x) N_J(x)\, \mathrm{d}\Omega \tag{45}$$

$$g_I = \int_\Omega N_I(x) \boldsymbol{\phi}^{Eh}(x)\, \mathrm{d}\Omega \tag{46}$$

From (43)–(46), the nodal values $\boldsymbol{\phi}_I$ corresponding to any element-based design described by $\boldsymbol{\phi}^{Eh}$ (given by (40)) can be obtained. Therefore for any element-based design there exists a corresponding nodal-based design.

Similarly, an inverse projection can be defined by (40) with

$$\boldsymbol{\phi}_\alpha^e = \boldsymbol{\phi}^{Nh}(\mathbf{x}_\alpha^e) \tag{47}$$

So any nodal-based design has an element-based dual. This duality is illustrated in Figure 4. Although a duality exists between the C^0 and C^1 designs as described above, this does not

Copyright © 2003 John Wiley & Sons, Ltd.

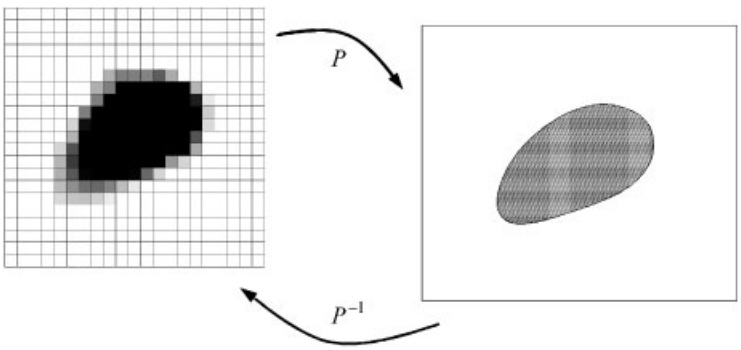

Figure 4. Projection between element-based design and nodal-based design.

imply that the solutions will have identical stability properties. In fact, the results obtained here indicate that the proposed method has significantly different stability properties.

This duality presents the possibility of some potentially useful algorithmic options. For examples, it may be possible to switch from nodal-based design to element-based design to check whether the former has missed a minimum because of limitations on the design space. Similarly, the projection (44) can be invoked at any step to obtain a smoother design.

5. GENERALIZATION TO DESIGN OF COMPOSITES

We describe next the formulation of some problems in the design of composites. Design of composites has previously considered in Reference [21]. Problems concerned with extreme materials including composites with extreme thermal expansion coefficients and smart composite materials have been considered in References [22] and [23], respectively. We consider here the design of a two-material composite. The design space Ω_{des} is a rectangle which corresponds to a representative volume element. Let the volumes occupied by materials A and B be denoted by Ω_A and Ω_B, respectively, and denote the union of the interfaces between Ω_A and Ω_B by Γ_{int}. The interfaces between the materials are specified by $\boldsymbol{\phi}(\mathbf{x})=0$ and we define that

$$\begin{aligned} \boldsymbol{\phi}(\mathbf{x}) &= 0 \quad \text{on } \Gamma_{\text{int}} \\ \boldsymbol{\phi}(\mathbf{x}) &> 0 \quad \text{in } \Omega_A \\ \boldsymbol{\phi}(\mathbf{x}) &< 0 \quad \text{in } \Omega_B \end{aligned} \tag{48}$$

The material property of the composites in the design space can then be written as

$$\mathbf{C}(\mathbf{x}) = \mathbf{C}_B + (\mathbf{C}_A - \mathbf{C}_B)H(\boldsymbol{\phi}(\mathbf{x})) \tag{49}$$

where $\mathbf{C}_A$ and $\mathbf{C}_B$ are the elasticity matrices of materials A and B, respectively.

The implicit function is discretized as before by shape functions (14). The displacement field requires extra terms to account for the discontinuity in the strains and stresses, so we

Copyright © 2003 John Wiley & Sons, Ltd.

approximate the displacement field by

$$\mathbf{u}(\mathbf{x}) = \sum_I N_I(\mathbf{x})\mathbf{u}_I + \sum_{I \in S} N_I(\mathbf{x})|\boldsymbol{\phi}(\mathbf{x})|\mathbf{q}_I \tag{50}$$

where S is the set of nodes whose support is crossed by the interface Γ_{int} and $\mathbf{q}_I$ are additional nodal parameters, see Belytschko *et al.* [24] and Sukumar *et al.* [25]. The above is a local partition of unity enrichment; see Babuška and Melenk [26] and Chessa *et al.* [27]. Note that the enrichment is also expressed in terms of the implicit function.

We impose a volume constraint that the volume of material A is fixed to V_0^A, i.e.

$$\int_{\Omega_{\text{des}}} H(\boldsymbol{\phi}(\mathbf{x}))\,\mathrm{d}\Omega = V_0^A \tag{51}$$

For simplicity we consider the problem of maximizing the stiffness. The formulation is now similar to the preceding. As before, the key steps are the nodal interpolation of $\boldsymbol{\phi}(\mathbf{x})$ and the regularization of the step function; the same regularization was used.

6. EXAMPLES

Except where noted, all examples were solved with 4-node quadrilateral structured meshes with bilinear displacement fields and $\alpha = 0.2$, $l = 0.05$. In elements away from the boundary, 2×2 quadrature was used. In elements where $|\boldsymbol{\phi}| \neq \alpha$ i.e. near a boundary, 3×3 quadrature was used. If not mentioned, the material parameters are: Young's modulus $E = 1000.0$ and Poisson's ratio $v = 0.3$. Plane strain is assumed and the loading is $P = 1.0$.

6.1. *Cantilever beam loaded on the right side*

The problem is defined in Figure 5. The displacement is constrained to vanish along AB and a load is applied as shown over a surface that is 0.2 in depth (and of unit width). The dimensions of design domain are: length $L = 8.0$, width $W = 5.0$. The volume constraint is $V_0 = 0.4V_{\text{des}}$.

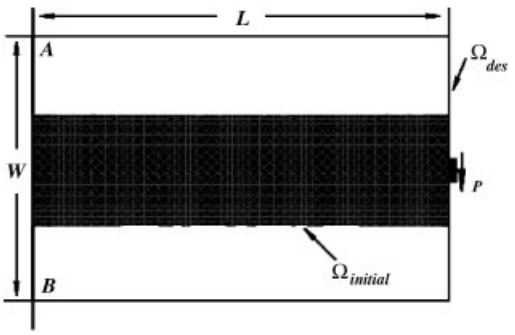

Figure 5. Definition of the problem 6.1.

Copyright © 2003 John Wiley & Sons, Ltd.

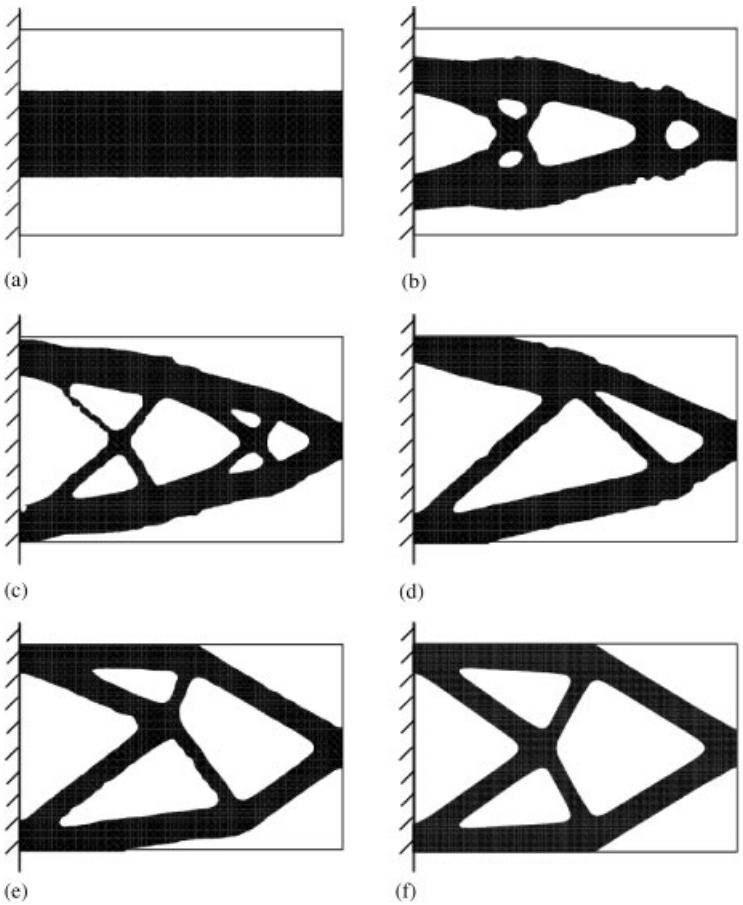

Figure 6. Process of optimization for cantilever beam loaded on the right side: (a) initial structure; (b) step 22; (c) step 40; (d) step 77; (e) step 105; and (f) final design.

Here, the left side is fixed and a 40×25 mesh is used. Figure 6 shows the intermediate shapes during the process of optimization, the final optimal structure is shown in Figure 6(f). It can be seen that the material moves rapidly from the centre where it is first located. Furthermore, the boundaries merge and holes are developed during the optimization procedure. The distribution of the von Mises effective stress of the optimal structure is shown in Figure 7.

Figure 8 is the optimal design from Sigmund's 99 line matlab code [15]. Because the density variable was used, the boundary of optimal structure is not as clear and smooth as the result which is shown in Figure 6(f). However, the design is otherwise identical.

We ran the optimization with various meshes for the same α and l. The minimum mean compliances are given in Table I. The values of C_{mean} for the different meshes are shown in Figure 9. It can be seen that the mean compliance converges to the final value quite rapidly for all of the meshes except the coarsest mesh. However, the final topology that is shown

Copyright © 2003 John Wiley & Sons, Ltd.

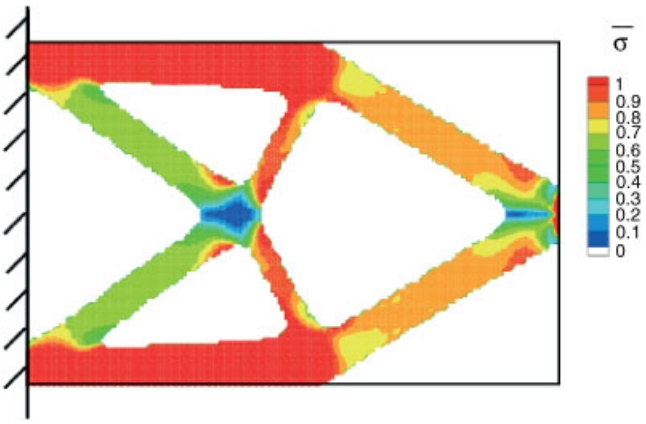

Figure 7. Von Mises effective stress distribution for final design.

Figure 8. Optimal structure by method of Sigmund [15].

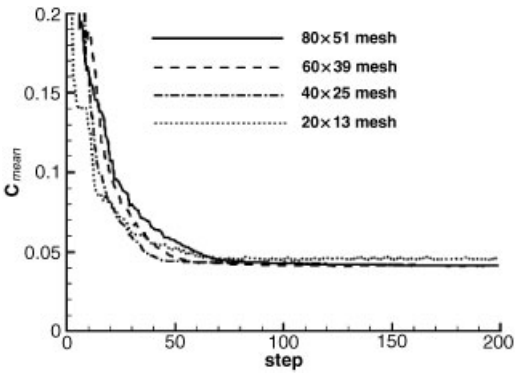

Figure 9. The mean compliance during the process of optimization.

Table I. The minimal mean compliance for different meshes.

Meshes	20×13	40×25	50×31	60×39	70×45	80×51
C_{mean}	0.0450	0.0415	0.0414	0.0410	0.0411	0.0411

in Figure 6 requires a large number of additional steps. The values of α and l do not effect the minimal mean compliance much. We found that the larger smoothing length l will result in faster convergence so that a larger smoothing length is suggested for fine meshes. It is apparent that a 40×25 mesh is sufficient to obtain good results. From Figures 6 and 9 it can be seen that while the compliance is almost unchanged from step 77, the topology still changes significantly. Evidently, certain components of the gradient of the objective function are very small in the vicinity of the optimum.

Copyright © 2003 John Wiley & Sons, Ltd.

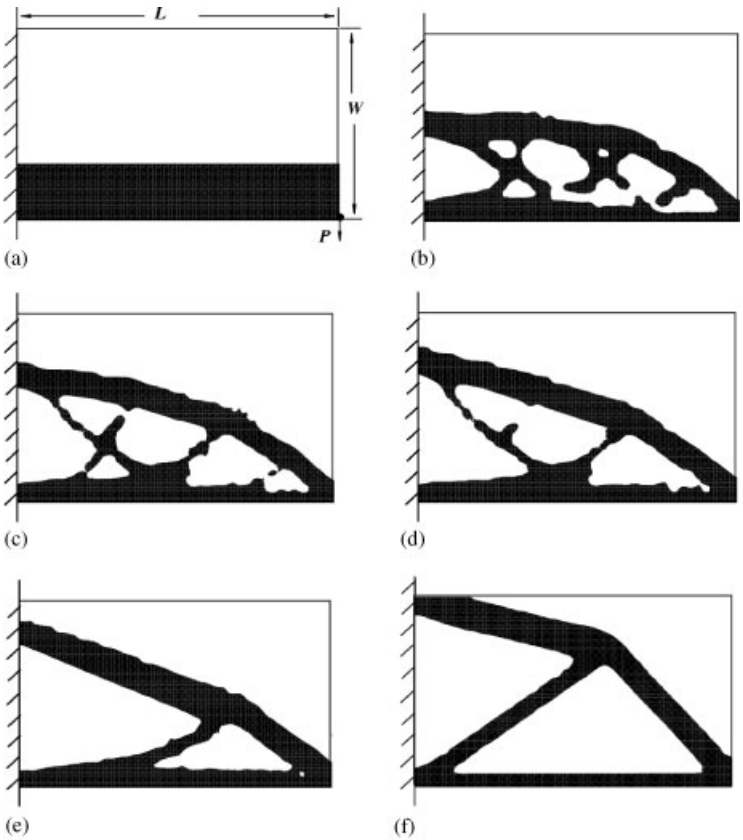

Figure 10. Process of optimization for initial design 1: (a) initial design 1; (b) step 25; (c) step 50; (d) step 70; (e) step 100; and (f) final design.

The 9-node element is also studied here with a 40×25 mesh. 4×4 quadrature is used with C^1 shape function. It gives an identical minimal mean compliance and identical final design.

6.2. *Cantilever beam loaded at the right bottom*

The same design domain is considered for a cantilever beam with the load applied on the bottom right corner. Two different initial structures were used as shown in Figures 10 and 11. The volume constraint is $V_0 = 0.3V_{\text{des}}$. Figures 10 and 11 also show the optimization processes for the different initial shapes. It can be seen that although the initial shapes are different, the optimal structures are identical. Again, the method is able to open holes, merge surfaces and generate new surfaces in the optimization process.

6.3. *Cantilever beams with a fixed hole*

We also consider a cantilever beam with a fixed hole; this problem was previously studied by Sigmund [15]. As shown in Figure 12, the dimensions of cantilever beam are: $L = 9.0$ and

Copyright © 2003 John Wiley & Sons, Ltd.

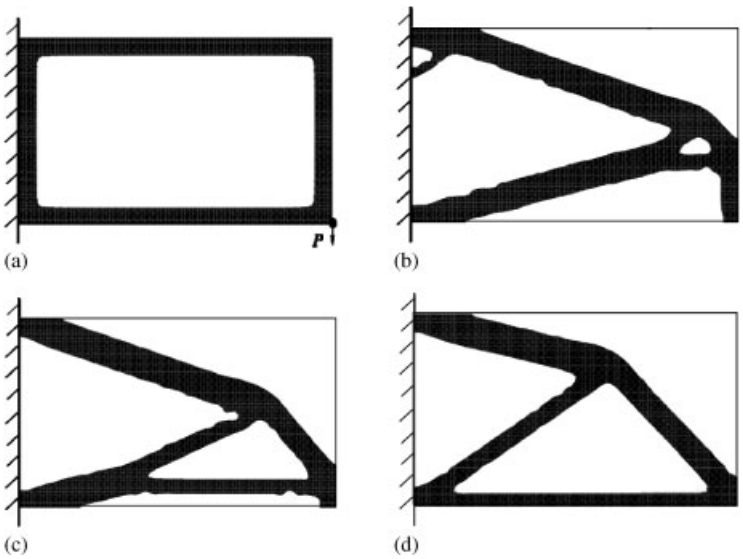

Figure 11. Process of optimization for initial design 2: (a) initial design 2; (b) step 30; (c) step 100; and (d) final design.

$W = 6.0$. The radius of the hole is 2.0 and its centre is at $(3.0, 3.0)$. The volume of material is $V_0 = 0.5V_{\text{des}}$. The same loadings are considered as examples 6.1 and 6.2. Figure 13 shows the final optimal designs for different loadings. The final design of Figure 13(a) is almost identical to that of Sigmund [15].

6.4. Composite material

In the following, the topology optimization method is used to design a composite material. In this problem, the two materials are designated by A and B. The parameters are: Young's modulus $E_A = 2E_B = 1.0$ and Poisson's ratio $v_A = v_B = 0.3$. The volume constraint is $V_0^A = 0.42V_{\text{des}}$. The topology optimization was applied to a square based cell, each of which is required to contain a hole of radius $0.25L$, where L is the length of the side. 30×30 and 45×45 element meshes are used. The initial distribution of these two materials is shown in Figure 14 with uniaxial compression $\sigma = 1.0$ applied in the y-direction.

The topology optimization procedure is applied on the base cell with periodic boundary conditions. Figure 15 shows the final distribution of the materials. It can be seen that in the optimum design, the material shifts as much as possible away from the hole so that the stiffest possible continuous member remains.

6.5. Centre-loaded beam

This problem is well known to be subject to instabilities in the Bendsøe–Kikuchi type methods, see Jog and Haber [28]. The problem description is given in Figure 16. The volume constraint is $V_0 = 0.6V_{\text{des}}$. The design obtained by present method is shown in Figure 17. As can be seen, the design is quite smooth and free of any signs of instability.

Copyright © 2003 John Wiley & Sons, Ltd.

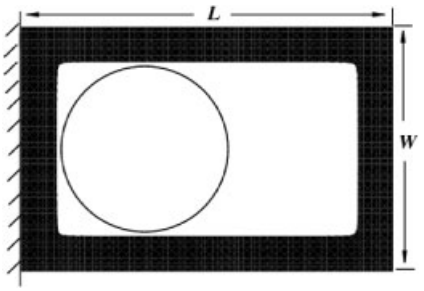

Figure 12. Cantilever beam with a fixed hole.

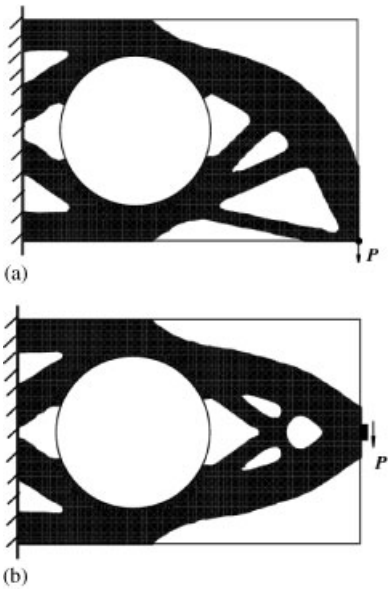

Figure 13. Optimized shape under two different loadings.

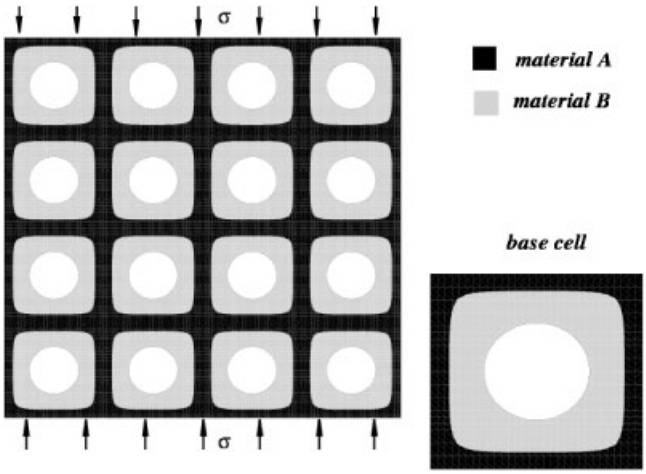

Figure 14. Initial design of composite with holes.

7. CONCLUSIONS

A method for topology optimization based on implicit function description of the surface of the design has been described. The implicit function is described in terms of nodal variables and C^0 finite element shape functions. The implicit function is viewed as the design variable

Copyright © 2003 John Wiley & Sons, Ltd.

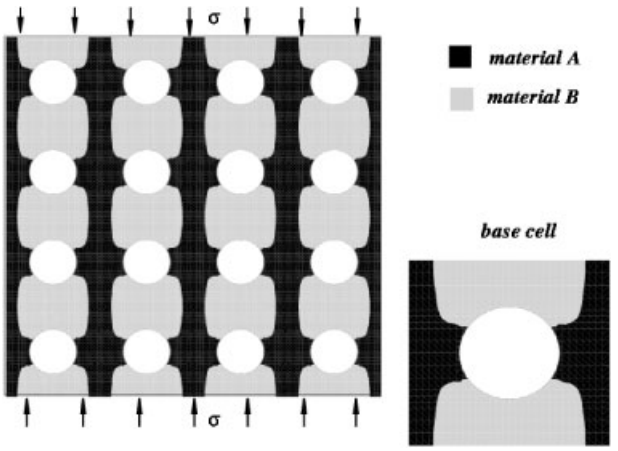

Figure 15. Optimal design of composite with holes.

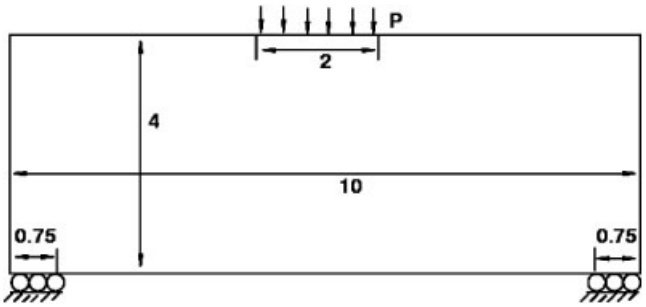

Figure 16. Centre-loaded beam.

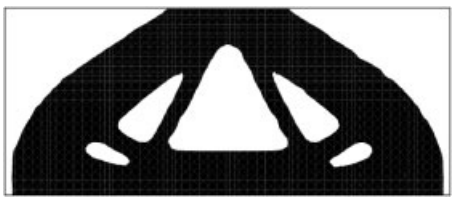

Figure 17. Final design of centre-loaded beam.

and the optimization problem can then be posed as a mathematical programming problem in terms of the nodal displacements and the nodal values of the implicit function.

The method is closely related to the homogenization methods of Bendsøe and Kikuchi [10], and we have proposed a duality between the methods. However, the numerical properties appear to be different. Remarkably, no oscillatory results were observed as is often found in the element-based methods. Indeed, the results converged smoothly to smooth results. At first glance, one may try to explain the different stability characteristics by the analogy to the Stokes

Copyright © 2003 John Wiley & Sons, Ltd.

problem proposed by Jog and Haber [28]. According to their proposal, the density in the design problem corresponds to the pressure in the Stokes problem. The Bendsøe–Kikuchi method thus corresponds to the discrete Stokes problem with a constant pressure, bilinear velocity quadrilateral element. However, the Stokes problem element corresponding to the optimization element for our method, which is the continuous bilinear pressure, bilinear velocity element is also unstable, see Hughes [29]. Thus the stability properties apparently involve additional or different factors. On the other hand, our method may possess an instability that was not revealed in these examples.

The method shares many features with the homogenization method of Bendsøe and Kikuchi [10]; a structured mesh is used on the design space and the topology is obtained by finding the stationary value with respect to a smoothing variable. In the Bendsøe–Kikuchi approach, the smoothing variable is the size of the hole in the element, in this case the regularized step function. However, the design parameters in the Bendsøe–Kikuchi approach are element related, whereas the shape here is piecewise continuous. This may account for the greater smoothness and stability of this method. The present method makes no recourse to any microstructural variables. Instead, the shape is directly described by implicit functions and uses regularization of the step function.

It would be quite straightforward to add h-adaptivity as p-adaptivity in the present method. In addition, by using features from previously developed extended finite element method, we are able to treat material interfaces with accuracy.

The methodology undoubtedly has limitation in the geometries that can be treated, for it is known that implicit surface definitions can lead to difficulties at corners. We have not encountered these here. It appears that in the realm of problems we have exploited, optimum shapes are quite smooth so the interpolation by finite element shape functions has proved quite robust.

ACKNOWLEDGEMENTS

We gratefully acknowledge the grant support from the NASA University Research, Engineering and Technology Institute on Bio Inspired Materials (BIMat) under award No. NCC-1-02037 and the Office of Naval Research.

REFERENCES

1. Moës N, Dolbow J, Belytschko T. A finite element method for crack growth without remeshing. *International Journal for Numerical Methods in Engineering* 1999; **46**(1):131–150.
2. Belytschko T, Parimi C, Moës N, Sukumar N, Usui S. Structured extended finite element methods for solids defined by implicit surfaces. *International Journal for Numerical Methods in Engineering* 2003; **56**(4):609–635.
3. Schmit LA. Structural design by systematic synthesis. 105, *Proceedings of the 2nd ASCE Conference on Electronic Computation*, vol. 105. ASCE: New York, 1960.
4. Fox RL. Constraint surface normals for structural synthesis techniques. *AIAA Journal* 1965; **3**(8):1517.
5. Prager W, Taylor JE. Problems of optimal structural design. *Journal of Applied Mechanics* (ASME) 1968; **35**:102.
6. Prager W. A note on discretized Michell structures. *Computer Methods in Applied Mechanics and Engineering* 1974; **3**(3):349.
7. Svanberg K. Optimal geometry in truss design. In *Foundations of Structural Optimization*: *A Unified Approach*. Morris AJ (ed.). Wiley: New York, 1982.
8. Zienkiewicz OC, Campbell JS. Shape optimization and sequential linear programming. In *Optimal Structural Design*. Wiley: New York, 1973.

Copyright © 2003 John Wiley & Sons, Ltd.

9. Haftka RT, Grandhi RV. Structural shape optimization—A survey. *Computer Methods in Applied Mechanics and Engineering* 1986; **57**(1):91.
10. Bendsøe MP, Kikuchi N. Generating optimal topologies in optimal design using a homogenization method. *Computer Methods in Applied Mechanics and Engineering* 1988; **71**:197.
11. Bendsøe MP. Optimal shape design as a material distribution problem. *Structural Optimization* 1989; **1**:193.
12. Zhou M, Rozvany GIN. The COC algorithm, part II: topological, geometry and generalized shape optimization. *Computer Methods in Applied Mechanics and Engineering*. 1991; **89**:197.
13. Mlejnek HP. Some aspects of the genesis of structures. *Structural Optimization* 1992; **5**:64.
14. Bendsøe MP. *Optimization of Structural Topology*, *Shape and Material*. Springer: New York, 1995.
15. Sigmund O. A 99 line topology optimization code written in Matlab. *Structural and Multidisciplinary Optimization* 2001; **21**:120.
16. Sethian JA, Wiegmann A. Structural boundary design via level set and immersed interface methods. *Journal of Computational Physics* 2000; **163**(2):489.
17. Belytschko T, Black T. Elastic crack growth in finite elements with minimal remeshing. *International Journal for Numerical Methods in Engineering* 1999; **45**(5):601.
18. Dolbow J, Moës N, Belytschko T. Discontinuous enrichment in finite element with a partition of unity method. *Finite Elements in Analysis and Design* 2000; **36**(3–4):235.
19. Fletcher R, Reeves CM. Function minimization by conjugate gradients. *Computer Journal* 1964; **7**:149.
20. Belytschko T, Liu WK, Moran B. *Nonlinear Finite Elements for Continua and Structures*. Wiley: New York, 2000.
21. Sigmund O. Materials with prescribed constitutive parameters: an inverse homogenization problem. *International Journal of Solids and Structures* 1994; **31**(17):2313.
22. Sigmund O, Torquato S. Composites with extremal thermal expansion coefficients. *Applied Physics Letters* 1996; **69**(21):3203.
23. Sigmund O, Torquato S. Design of smart composite materials using topology optimization. *Smart Materials and Structures* 1999; **8**:365.
24. Belytschko T, Moës N, Usui S, Parimi C. Arbitrary discontinuities in finite elements. *International Journal for Numerical Methods in Engineering* 2001; **50**(4):993.
25. Sukumar N, Chopp DL, Moës N, Belytschko T. Modeling holes and inclusions by level sets in the extended finite element method. *Computer Methods in Applied Mechanics and Engineering* 2001; **190**(46–47):6183.
26. Babuška I, Melenk JM. The partition of unity method. *International Journal for Numerical Methods in Engineering* 1997; **40**(4):727.
27. Chessa J, Wang H, Belytschko T. On the construction of blending elements for local partition of unity enriched finite elements. *International Journal for Numerical Methods in Engineering* 2003; **57**:1015–1038.
28. Jog CS, Haber RB. Stability of finite element models for distributed-parameter optimization and topology design. *Computer Methods in Applied Mechanics and Engineering* 1996; **130**:203.
29. Hughes TJR. *Finite Element Method—Linear Static and Dynamic Finite Element Analysis*. Prentice-Hall: Englewood Cliffs, 1987.

Copyright © 2003 John Wiley & Sons, Ltd.